Aeroacoustics Conferences
June 14-17, 2022, Southampton, UK
28th AIAA/CEAS Aeroacoustics 2022 Conference

10.2514/6.2022-2866

Check for updates

Mach number dependence of tone generation in impinging round jets

Mathieu Varé* and Christophe Bogey†
Univ Lyon, École Centrale de Lyon, INSA Lyon, Université Claude Bernard Lyon I, CNRS
Laboratoire de Mécanique des Fluides et d'Acoustique, UMR 5509
F-69134 Ecully, France

The Mach number dependence of the tones generated by round jets impinging on a flat plate, due to aeroacoustic feedback loops establishing between the jet nozzle and the plate, are investigated using large-eddy simulations. Six jets at Mach numbers varying from 0.6 to 1.1 and a nozzle-to-plate distance of 8 nozzle radii are considered. For $M = 0.6$, the upstream sound radiation is broadband and weak, which suggests the absence of marked feedback phenomena. For higher Mach numbers, it is tonal and intense, highlighting the establishment of feedback loops between the nozzle and the plate. Tones are present at the same frequencies in both the velocity spectra in the shear-layer and the near-nozzle acoustic spectra, highlighting a coupling between the jet flow structures and the upstream-propagating pressure waves. For $M \leq 1$, the dominant tone is associated with an axisymmetric oscillation mode of the jet, whereas for $M = 1.1$, it is related to an helical mode, showing that the jet azimuthal structure is affected by the Mach number. For both azimuthal modes, standing-wave patterns are found inside the jets in the pressure amplitude fields at the tonal frequencies, indicating interactions between upstream and downstream-propagating waves. Moreover, the tone frequencies decrease with the Mach number. They are located in the frequency ranges of the upstream-travelling guided jet waves, indicating that these waves close the feedback loop in all cases. As for the amplitude of the tones, it increases by about 45 dB between $M = 0.6$ and 1, which is much higher than the rise predicted by the M^8 law. It is then reduced by 15 dB for $M = 1.1$, suggesting a weaker resonance for this jet.

Downloaded by Christophe Bailly on June 16, 2022 | http://arc.aiaa.org | DOI: 10.2514/6.2022-2866

I. Introduction

Strong acoustic tones can be generated by jets impinging on a flat plate. Such tones have been observed for high subsonic jets in many experiments, such as those of Wagner [1], Neuwerth [2], Preisser [3], Ho & Nosseir [4, 5] and Powell [6]. Later, they have been also found for supersonic impinging jets in the experiments of Norum [7], Tam & Norum [8] and Henderson *et al.* [9] and in the simulations of Gojon & Bogey [10] and Bogey & Gojon [11], for instance. Similar tones are emitted by subsonic and supersonic jets impinging on a perforated plate [12–14]. They are produced by a feedback loop establishing between the nozzle and the plate. The downstream part of this loop consists of the well-known Kelvin-Helmholtz instability waves, related to the formation and convection of coherent structures in the jet mixing layers. The upstream part is formed by upstream-propagating guided jet waves [15], defined by specific dispersion relations and classified into modes depending on their radial and azimuthal structures. Such waves play a role in other resonance phenomena, for example in screech noise generation mechanisms [16, 17] and jet-flap interactions [18, 19]. They are also involved in the generation of tones in the near-nozzle pressure field of free jets [20–22]. The properties of the guided jet waves and of the feedback loop depend on the jet Mach number. In particular, for impinging jets, Tam & Ahuja [15] observed that no feedback loop establishes for Mach numbers M lower than 0.7. Moreover, the azimuthal structure of the jets varies with the Mach number. Indeed, based on the work of Tam & Ahuja [15], Panickar & Raman [23] showed that only an axisymmetric feedback mode is found for $M < 0.89$ and that helical feedback modes exist for higher Mach numbers. Furthermore, the effects of the Mach number on the feedback frequencies were studied experimentally by Jaunet *et al.* [24]. These frequencies are organized into stages as the Mach number increases, which is typical of resonance phenomena. They lie in the allowable frequency ranges of the upstream-travelling guided jet waves, suggesting a closure of the feedback loop by these waves.

*Postdoctoral fellow, mathieu.vare@ec-lyon.fr
†CNRS Research Scientist, AIAA Senior Member & Associate Fellow, christophe.bogey@ec-lyon.fr

Copyright © 2022 by Mathieu Varé and Christophe Bogey. Published by the American Institute of Aeronautics and Astronautics, Inc., with permission.

However, several questions remain about the influence of the Mach number on the feedback mechanisms in impinging jets. Among others, it is still unclear whether the nature of the dominant tone is axisymmetric or helical for jets at Mach numbers higher than 0.89, for which both oscillation modes are possible. Moreover, the link between the staging of the tone frequencies with the Mach number and the properties of the upstream-propagating guided jet waves closing the loop still needs to be clarified. Furthermore, the effects of the jet velocity on the intensity of the tones have not been studied thoroughly.

In the present work, the large-eddy simulations (LES) of six impinging round jets at Mach numbers varying from 0.6 to 1.1 are performed in order to investigate the effects of the Mach number on the feedback mechanism establishing between the nozzle and the plate. The jets are at a Reynolds number of 10^5 and are initially highly disturbed. They impinge on a flat plate located at a distance L of 8 nozzle radii from the nozzle exit. The first objective of this study is to observe the establishment of feedback loops between the nozzle and the plate. For that purpose, the flow and acoustic fields are detailed. In particular, the velocity and near-nozzle pressure spectra are examined to determine tonal frequencies. The contributions of the first two azimuthal modes are explored to study the oscillation modes of the jets. The frequencies and the axisymmetric or helical nature of the tones are compared with the properties of the free-stream upstream-propagating guided jet waves with the aim of highlighting the role of these waves in the feedback mechanisms. The Mach number variations of the tone frequencies and amplitudes are detailed. Finally, the structures of the pressure fields at the peak frequencies are investigated.

This paper is organized as follows. The jet parameters and numerical methods used in the LES are presented in section II. The results of the simulations are detailed in section III. Finally, concluding remarks are given in section IV.

II. Parameters

A. Jet parameters

The six jets computed in this work have Mach numbers of $M = 0.6, 0.75, 0.8, 0.9, 1$ and 1.1 and a Reynolds number $Re_D = u_j D/\nu$ of 10^5, where u_j is the jet velocity, D is the nozzle diameter and ν is the air kinematic viscosity. They originate at $z = 0$ from a cylindrical nozzle of radius r_0 and length $2r_0$, and are at ambient pressure and temperature $p_0 = 10^5$ Pa and $T_0 = 293$ K. They impinge on a plate located $L = 8r_0$ downstream of the nozzle exit, as in the experiments of Jaunet *et al.* [24]. At the nozzle inlet, a Blasius laminar boundary-layer profile with a thickness of $\delta = 0.15r_0$ is imposed for the velocity. Vortical disturbances uncorrelated in the azimuthal direction are added in the boundary layer at $z = -r_0$ to create velocity fluctuations at the nozzle exit, using a procedure described in Bogey *et al.* [25]. The profiles of mean and rms axial velocities obtained at the nozzle exit for the six jets are represented in figure 1. They are very similar to each other. In figure 1(a), the mean velocity profiles resemble the Blasius laminar boundary-layer profile at the inlet, while the turbulent intensities reach a peak value of 9% at $r = 0.97r_0$ in figure 1(b). Therefore, the jets are initially highly disturbed.

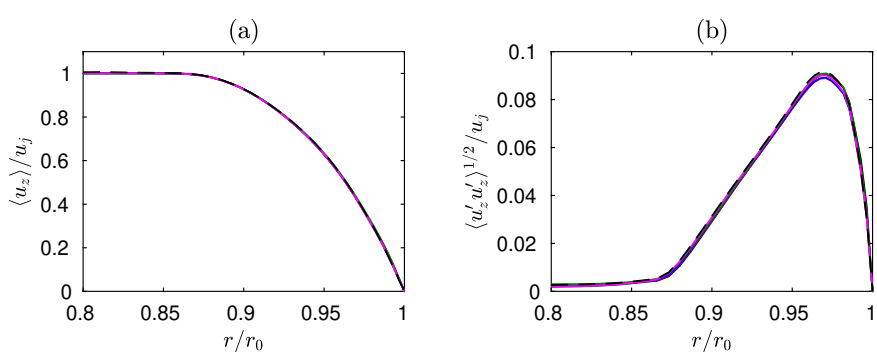

Fig. 1 Nozzle-exit radial profiles of (a) mean axial velocity $\langle u_z \rangle / u_j$ and (b) axial turbulence intensity $\langle u'_z u'_z \rangle^{1/2} / u_j$; —— $M = 0.6$, —— $M = 0.75$, —— $M = 0.8$, —— $M = 0.9$, —— $M = 1$ and - - - $M = 1.1$

Downloaded by Christophe Bailly on June 16, 2022 | http://arc.aiaa.org | DOI: 10.2514/6.2022-2866

Downloaded by Christophe Bailly on June 16, 2022 | http://arc.aiaa.org | DOI: 10.2514/6.2022-2866

B. Numerical methods

The numerical setup is the same as that of very recent LES of subsonic [14] and supersonic [26, 27] impinging jets. The unsteady compressible Navier-Stokes equations are solved in cylindrical coordinates (r, θ, z) using an OpenMP based in-house solver. A second-order, six-stage Runge-Kutta algorithm [28] is employed for time-integration and the spatial derivatives are computed with eleven-point low-dispersion finite-difference schemes [29]. At the end of each time step, a selective filtering is applied to remove grid-to-grid oscillations [28]. This filter also acts as a subgrid-scale model ensuring the relaxation of turbulent kinetic energy near the grid cut-off frequency [30]. No-slip and adiabatic wall conditions are imposed to the plate and nozzle walls. In order to handle possible shocks created by the jet impingement in the jet potential core, a damping procedure using a dilatation-based shock detector and a second-order filter is used to remove Gibbs oscillations in the vicinity of shocks for $z \geq 3r_0$ [31]. The radiation boundary conditions of Tam & Dong [32] are implemented at the radial and lateral boundaries of the computational domain. They are associated with sponge zones combining grid stretching and Laplacian filtering to prevent significant spurious reflections [33]. The method of Mohseni & Colonius [34] is applied to treat the singularity on the jet axis. The closest point to the axis is located at $r = \Delta r/2$, where Δr is the radial mesh size near the jet axis. The azimuthal derivatives near the jet axis are evaluated with fewer points than permitted by the grid to increase the time step of the simulations [35]. More precisely, the effective azimuthal resolution near the origin of the polar coordinates is reduced down to $2\pi/16$.

C. Computational parameters

The same mesh grid is used for the six simulations. It is similar to that employed in a very recent simulation of a jet at a Mach number of 0.9 impinging on a flat plate at $L = 6r_0$ [14]. More precisely, the numbers of points in the radial, azimuthal and axial directions are equal to 559, 1024 and 1124, respectively, which yields a total number of 640 million points. The grid extends out to $r = 15r_0$ in the radial direction and down to $z = 8r_0$ in the axial direction. The radial mesh spacing, shown in figure 2(a), is equal to $\Delta r = 0.014r_0$ on the jet centerline and decreases down to $\Delta r = 0.0036r_0$ at $r = r_0$ in the shear layers. It then increases to reach a maximum value of $\Delta r = 0.075r_0$ for $r > 6.2r_0$, which leads to a Strouhal number $St = fD/u_j$ varying from 4.8 at $M = 1.1$ up to 8.9 at $M = 0.6$ for an acoustic wave with five points per wavelength. The axial mesh spacing Δz, in figure 2(b), is minimum and equal to $\Delta z = 0.0072r_0$ at the nozzle exit, and maximum and equal to $\Delta z = 0.012r_0$ between $z = 2r_0$ and $z = 6r_0$. Farther downstream, the axial mesh spacing is reduced down to $\Delta z = 0.0072r_0$ near the plate at $z = 8r_0$, as at the nozzle exit. The extremum values of the mesh spacings and the stretching rates in the axial and radial directions are the same as in the study of Bogey [36], where a grid convergency study was performed for a free jet with the same ejection conditions as the impinging jet at $M = 0.9$ of the present work. The results presented in this paper are obtained after simulation times of $1000r_0/u_j$ for all jets. During the simulations, density, velocity components and pressure along the jet axis at $r = 0$, along the lip line at $r = r_0$, on the surfaces at $r = 15r_0$, $z = -2r_0$, $z = 0$ and on the plate at $z = L$ are recorded at a sampling frequency enabling spectra to be computed up to $St = 12$. Density, velocities and pressure are also saved at the azimuthal angles $\theta = 0$, 90, 180 and 270 degrees at a halved frequency. The azimuthal Fourier coefficients of the density, pressure and velocity fields are also estimated up to the mode $n_\theta = 4$ for $0 \leq r \leq 15r_0$ and $0 \leq z \leq 8r_0$. The spectra are computed from these recordings and they are averaged in the azimuthal direction when possible.

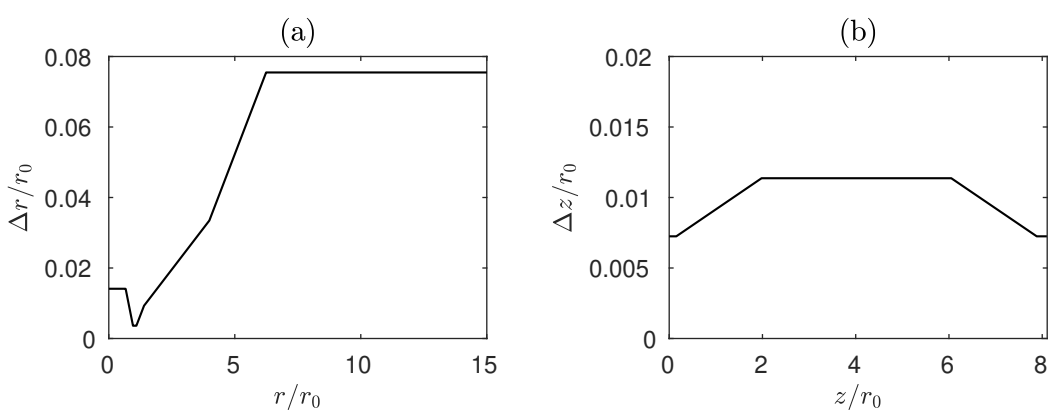

Fig. 2 Variations of (a) radial and (b) axial mesh spacings.

Downloaded by Christophe Bailly on June 16, 2022 | http://arc.aiaa.org | DOI: 10.2514/6.2022-2866

III. Results

A. Snapshots of the flow and acoustic fields

Snapshots of the vorticity norm in the flow and of the pressure fluctuations outside are presented in figure 3. For all jets, in the vorticity fields, the shear layers thicken with the axial distance due to the formation of large-scale vortical structures. The structures are convected down to the plate, where their impingement creates wall jets. Farther from the stagnation point, the wall jets spread radially and widen with the radial distance. In the pressure fields, high-frequency sound waves are found to be generated near the flat plate, notably in the wall jets, and to propagate in the upstream direction. For $M \geq 0.75$ in figures 3(b-f), intense low-frequency waves originating from the plate are also visible. They are produced by the impingement of the jet turbulent structures on the plate. Their wavefronts are periodically spaced, revealing tonal radiations. For Mach numbers between 0.8 and 1 in figures 3(c-e), no phase shift is observed between the two sides of the nozzle, indicating an axisymmetric pressure field. This is not the case for the jet at $M = 1.1$ in figure 3(f), which may be due to helical jet oscillations. As for the amplitudes of the pressure fluctuations, they are about 500 Pa for $M = 0.6$ and increase with the Mach number to reach a maximum for $M = 1$. In particular, they are of the order of 1000 Pa for the jets at $M \geq 0.9$.

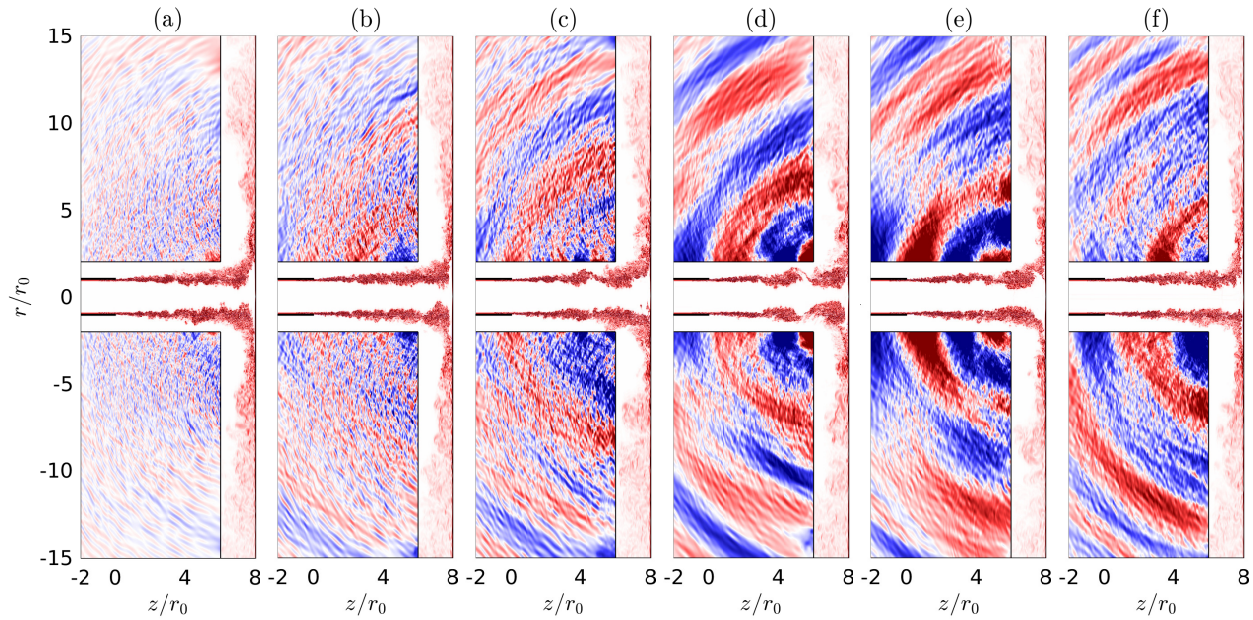

Fig. 3 Snapshots of vorticity norm in the flow and of pressure fluctuations outside in the (z, r) plane for (a) $M = 0.6$, (b) $M = 0.75$, (c) $M = 0.8$, (d) $M = 0.9$, (e) $M = 1$ and (f) $M = 1.1$. The color scales range from 0 to $15u_j/r_0$ for vorticity, from white to red, and between (a-c) $\pm 0.005p_0$ and (d-f) $\pm 0.01p_0$ for pressure, from blue to red.

B. Mean flow fields

The variations of the centerline mean axial velocity, of the shear-layer momentum thickness and of the axial turbulence intensity at $r = r_0$ are presented in figure 4. In figure 4(a), the centerline mean axial velocity is approximately equal to the exit velocity down to $z = 6.5r_0$ for the six jets. It decreases down to zero on the plate at $z = 8r_0$. For $M \geq 0.9$, velocity oscillations are found, due to the presence of compression cells in the potential cores of the jets. In figure 4(b), the shear-layer momentum thicknesses are comparable for all jets. They increase nearly linearly down to $z = 7r_0$ then more drastically between $z = 7r_0$ and $z = 7.8r_0$ because of the wall jet. As for the root-mean-square (r.m.s.) values of the axial velocity fluctuations along the nozzle-lip line, in figure 4(c), they increase very quickly between $z = 0$ and $z = 2r_0$ in all cases. For $z \geq 2r_0$, they do not vary much down to $z = 7r_0$. In this zone, the turbulent levels are highest for $M = 0.6$, with values around 17% of u_j, and lowest for $M = 0.9$, with values around 13% of u_j. Finally, they are reduced down to zero on the plate.

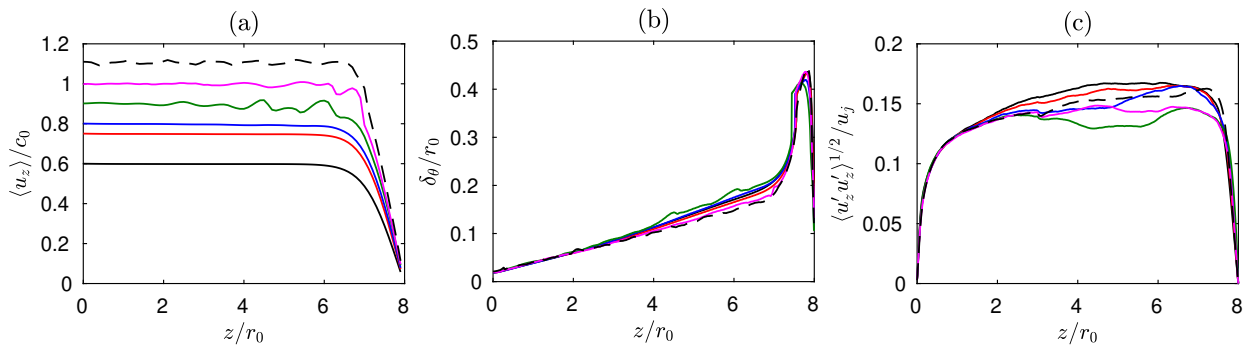

Fig. 4 Variations of (a) the centerline mean axial velocity $\langle u_z \rangle / c_0$, (b) the shear-layer momentum thickness δ_θ / r_0 and (c) the axial turbulent intensity $\langle u'_z u'_z \rangle^{1/2} / u_j$ at $r = r_0$ for —— $M = 0.6$, —— $M = 0.75$, —— $M = 0.8$, —— $M = 0.9$, —— $M = 1$ and - - - $M = 1.1$.

Downloaded by Christophe Bailly on June 16, 2022 | http://arc.aiaa.org | DOI: 10.2514/6.2022-2866

C. Velocity spectra

To study the development of the jet flow structures, the power spectral densities of the radial velocity fluctuations u'_r in the mixing layer at $r = r_0$ between the nozzle and the plate are displayed in figure 5. For $M \leq 0.9$ in figures 5(a-d), a spot of significant levels is observed for axial positions z between $4r_0$ and $7.5r_0$ at Strouhal numbers between 0.1 and 0.9. This spot is due to a broadband hump in the velocity spectra, associated with large coherent structures formed a few radii downstream of the nozzle exit. For $M = 1$ and 1.1 in figures 5(e,f), this spot is not visible anymore because of lower broadband levels. Moreover, for $M \geq 0.75$ in figures 5(b-f), the strongest levels are found along thin lines beginning at approximately $z = 2r_0$ for $M = 0.75$, 0.8 and 0.9, $z = r_0$ for $M = 1$, and $z = 3r_0$ for $M = 1.1$, and extending down to the plate. They are located at Strouhal numbers depending on the jet Mach number. More precisely, the Strouhal numbers of the lines are equal to 0.46, 0.54 and 0.61 for $M = 0.75$, to 0.51 and its first harmonic for $M = 0.8$, to 0.40 and its two first harmonics for $M = 0.9$, to 0.31 and its first harmonic for $M = 1$ and to 0.29, 0.46 and 0.66 for $M = 1.1$. These persistent peaks indicate the presence of tones in the velocity spectra, suggesting the establishment of aeroacoustic feedback loops between the nozzle and the plate. The jet shear layers thus appear to be forced by upstream-travelling waves closing the loops. The feedback loops and the upstream-propagating waves are investigated in the next sections.

In order to examine the forcing of the jet shear layers by the upstream-propagating waves, the spectra of the radial velocity fluctuations in the mixing layer and the contributions of the two first azimuthal modes to these spectra are computed near the nozzle-exit and near the plate. The spectra obtained near the nozzle lip, at $r = r_0$ and $z = 0.4r_0$, are represented in figure 6 as a function of the Strouhal number. For all jets, a broadband hump is observed for both modes around a Strouhal number of $St = 1.7$, which is close to the frequency $St_\theta = f\delta_\theta/u_j = 0.016$ of the most-amplified Kelvin-Helmholtz instability waves obtained using linear stability analysis [37]. For $M = 0.6$ in figure 6(a), no tones are observed in the velocity spectra, which is not the case for the jets at higher Mach numbers. For the latter jets, the tone frequencies are similar to those of the tones observed in the spectrograms of figure 5. The tones are associated with the axisymmetric mode $n_\theta = 0$ for $M = 0.75$ and 0.8 in figures 6(b,c), and with the axisymmetric and first helical modes for $M = 0.9$, 1 and 1.1 in figures 6(d,e,f). For $n_\theta = 0$, a tone is strongly dominating at $St = 0.61$ for $M = 0.75$ in figure 6(b), at $St = 0.51$ for $M = 0.8$ in figure 6(c), at $St = 0.40$ for $M = 0.9$ in figure 6(d) and at $St = 0.31$ for $M = 1$ in figure 6(e), whereas two strong tones are located at $St = 0.29$ and 0.66 for $M = 1.1$ in figure 6(f). Weak harmonics of the dominant tone are also observed for $M = 0.9$ and $M = 1$. For $n_\theta = 1$, a weak tone emerges at $St = 0.7$ and $St = 0.57$ for $M = 0.9$ and $M = 1$, respectively, and a tone of high amplitude appears at $St = 0.46$ for $M = 1.1$. For both modes, the frequencies of the dominant tones are three to five times lower than those of the most-amplified Kelvin-Helmholtz instability waves, suggesting again that the tones are caused by feedback loops establishing between the nozzle and the plate. This presence of low-frequency tones and high-frequency instability waves was also observed experimentally in the near-nozzle pressure spectrum of an impinging jet at a Mach number of 0.9 by Ho & Nosseir [4].

The spectra of the radial velocity fluctuations computed near the plate, at $r = r_0$ and $z = 7r_0$, are shown in figure 6 as a function of the Strouhal number. For all jets, a wide hump is visible around $St = 0.5$ for the two azimuthal modes. This low-frequency hump is linked to large vortical structures resulting from the growth of the shear layer turbulent structures with the axial distance. For $M \geq 0.75$ in figures 7(b-f), tones are found in the spectra for the same azimuthal modes and frequencies as for the spectra obtained at $z = 0.4r_0$, highlighting the development of coherent structures at

Downloaded by Christophe Bailly on June 16, 2022 | http://arc.aiaa.org | DOI: 10.2514/6.2022-2866

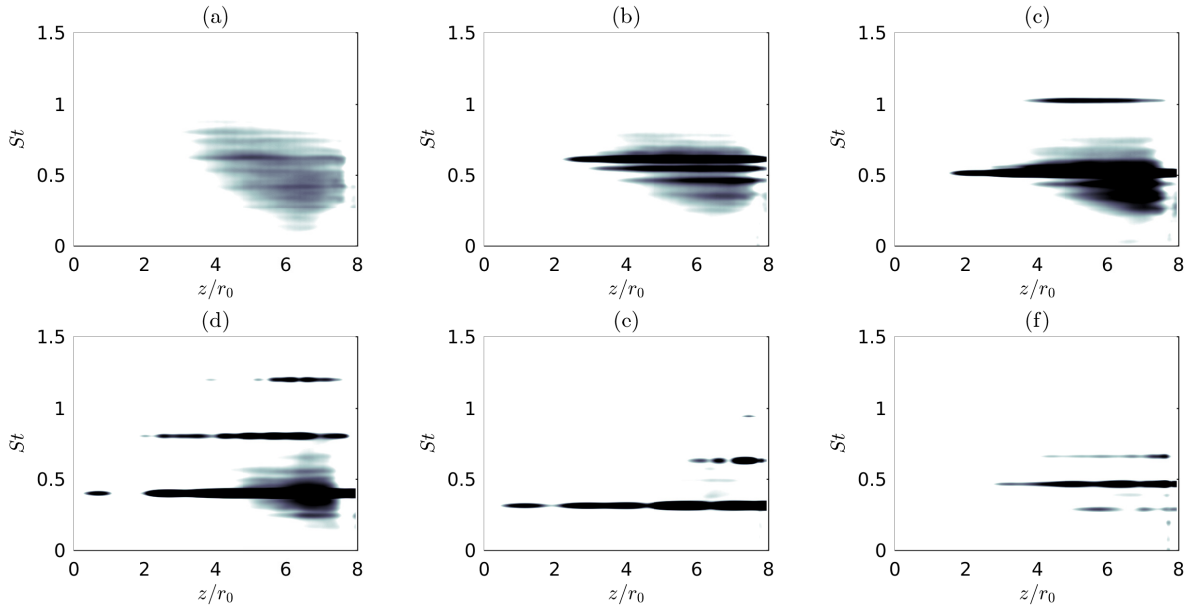

Fig. 5 Power spectral densities of the fluctuations of radial velocity u_r' normalized by the jet velocity u_j at $r = r_0$ between the nozzle and the plate for (a) $M = 0.6$, (b) $M = 0.75$, (c) $M = 0.8$, (d) $M = 0.9$, (e) $M = 1$ and (f) $M = 1.1$. The color scale is the same in all cases and spreads over 3 dB, from white to black.

the feedback frequencies down to the plate. For $M = 0.8$, 0.9 and 1 in figures 7(c,e), secondary tones are also visible at the harmonic frequencies of the dominant peak for the full signal and for $n_\theta = 0$.

D. Pressure spectra

The pressure spectra computed at $z = 0$ and $r = 1.5r_0$ near the nozzle are presented in figure 8. For $M = 0.6$ in figure 8(a), a broadband hump is observed around $St = 0.33$. No tone is visible, which suggests that there is no marked resonance phenomenon in this jet. This result is in agreement with previous experiments [1, 3, 4] highlighting that no feedback loop establishes for $M < 0.7$. For higher Mach numbers, tones emerge strongly. For the jet at $M = 0.75$ in figure 8(a), three tones 10 to 15 dB higher than the broadband noise are visible at Strouhal numbers of 0.46, 0.54 and 0.61. For the jet at $M = 0.8$, a dominant tone emerging by 20 dB is found at a Strouhal number of 0.51 and secondary peaks are observed at $St = 0.85$, 1.2 and 1.6. For the jet at $M = 0.9$ in figure 8(b), the pressure spectrum exhibits a strong tone 25 dB higher than the broadband noise at $St = 0.40$ and secondary tones emerging by about 10 dB at harmonic frequencies of the strongest tone and at $St = 0.7$ and 1. The spectrum for the jet at $M = 1$ displays a shape similar to that for the jet at $M = 0.9$, with a dominant tone at $St = 0.31$ and weaker peaks at harmonic frequencies of the dominant tone and at $St = 0.5$, 0.58, 0.82 and 1.25. For the jet at $M = 1.1$, three peaks 15 to 20 dB higher than the broadband levels are observed at $St = 0.29$, 0.46 and 0.66. For the jets at $M \geq 0.75$, the frequencies of the dominant tones are similar to the peak frequencies of the velocity spectra in section III.C, highlighting a coupling between the upstream-travelling waves and the flow structures.

The tones can be assumed to be produced by feedback loops establishing between the nozzle and the plate. The loops consist of two steps. During the first step, the coherent structures of the jet shear layers are convected downstream down to the plate, where their impingement generates acoustic waves. During the second step, these waves propagate upstream to the nozzle, exciting the mixing layer at the nozzle exit, which produces another coherent structure and closes the feedback loop. A model of prediction of the feedback frequencies was proposed by Ho & Nosseir [4]. In this model, the feedback period is considered as the sum of two characteristic times, namely the time of convection of the flow structures down to the plate and the time of propagation of the acoustic waves to the nozzle. The feedback frequency can thus be estimated by

$$f = \frac{N\langle u_c \rangle}{L(1 + M_c)} \tag{1}$$

Downloaded by Christophe Bailly on June 16, 2022 | http://arc.aiaa.org | DOI: 10.2514/6.2022-2866

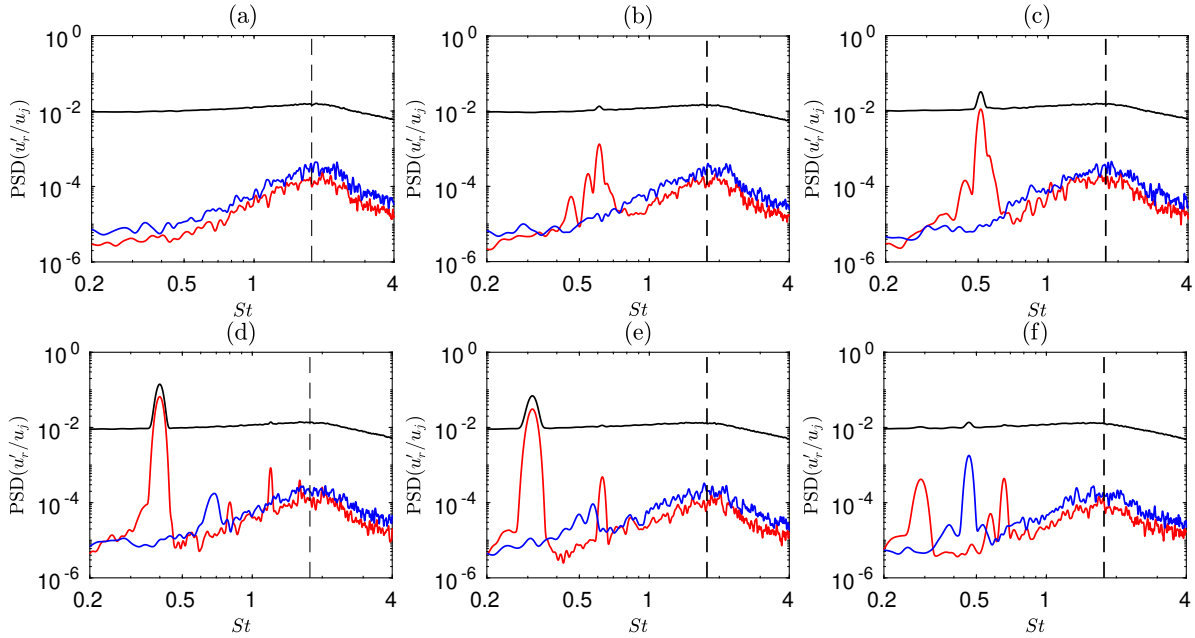

Fig. 6 Power spectral densities of the fluctuations of radial velocity u_r' at $r = r_0$ and $z = 0.4r_0$ for (a) $M = 0.6$, (b) $M = 0.75$, (c) $M = 0.8$, (d) $M = 0.9$, (e) $M = 1$ and (f) $M = 1.1$, —— full signal, —— $n_\theta = 0$ and —— $n_\theta = 1$, - - - $St_\theta = f\delta_\theta/u_j = 0.016$.

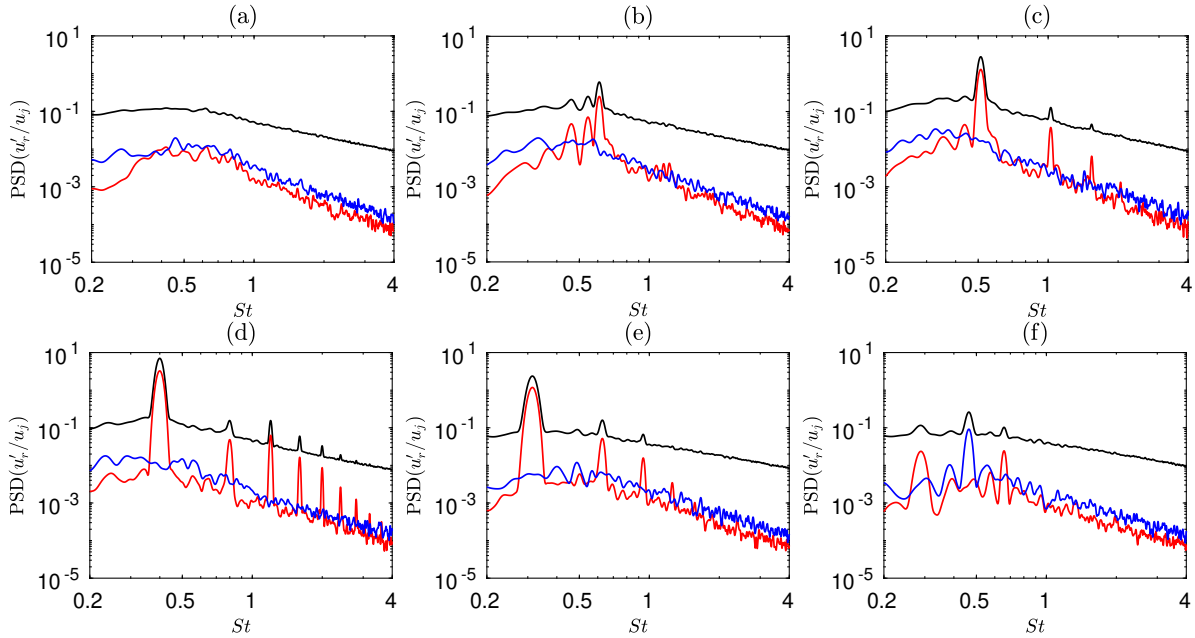

Fig. 7 Power spectral densities of the fluctuations of radial velocity u_r' at $r = r_0$ and $z = 7r_0$ for (a) $M = 0.6$, (b) $M = 0.75$, (c) $M = 0.8$, (d) $M = 0.9$, (e) $M = 1$ and (f) $M = 1.1$, —— full signal, —— $n_\theta = 0$ and —— $n_\theta = 1$.

where $\langle u_c \rangle$ is the mean convection velocity between the nozzle and the plate, $M_c = \langle u_c \rangle / c_0$ is the convection Mach number and N is an integer representing the order of the feedback mode. This integer N corresponds to the number of coherent structures between the nozzle and the plate. The feedback frequencies obtained by the model for different values of N using the classical approximation $\langle u_c \rangle = (2/3)u_j$ are given in table 1. For all jets at a Mach number $M \geq 0.75$, there exists a value of N giving a frequency close to that of the dominant peak in the pressure spectra, supporting the possibility of a feedback loop. The feedback order N decreases from 6 at $M = 0.75$ down to 3 at $M = 1$, then it increases up to 5 for $M = 1.1$.

Table 1 Strouhal numbers St_{LES} of the dominant tone frequencies in the LES and Strouhal numbers St_{model} predicted by the model of Ho & Nosseir [4] for a feedback mode N.

M	0.75	0.8	0.9	1	1.1
St_{LES}	0.61	0.51	0.40	0.31	0.46
N	6	5	4	3	5
St_{model}	0.67	0.54	0.42	0.3	0.48

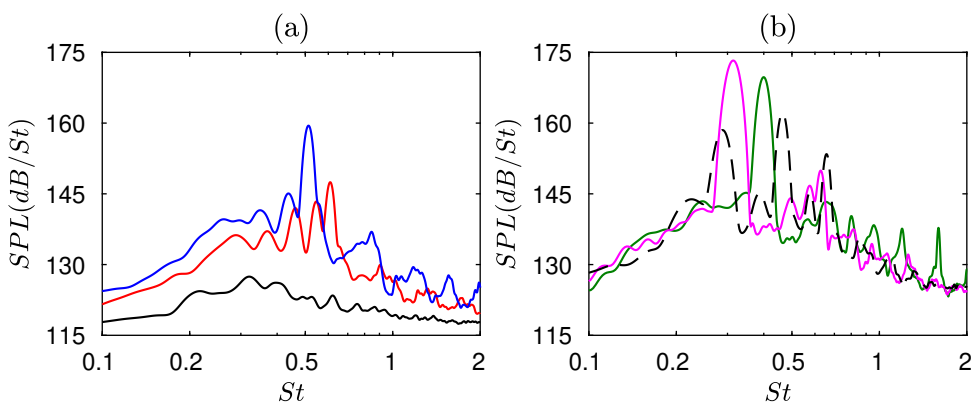

Fig. 8 Sound pressure levels (SPL) at $r = 1.5r_0$ and $z = 0$ for (a) —— $M = 0.6$, —— $M = 0.75$ and —— $M = 0.8$; (b) —— $M = 0.9$, —— $M = 1$ and - - - $M = 1.1$

To investigate the azimuthal structure of the pressure field near the nozzle for the six jets, the pressure spectra of figure 8 are represented alongside the contributions of the two first azimuthal modes for the six jets in figure 9. For the jet at $M = 0.6$ in figure 9(a), the low-frequency hump is linked to the axisymmetric mode $n_\theta = 0$. For the jets at Mach numbers between 0.75 and 1, in figures 9(b-e), the dominant tones are associated with $n_\theta = 0$. Secondary tones are also found for $n_\theta = 0$ at twice the frequencies of the dominant tones. Small peaks appear for the mode $n_\theta = 1$ at $St = 0.91$ for $M = 0.75$, $St = 0.84$ for $M = 0.8$, $St = 0.7$ for $M = 0.9$ and $St = 0.57$ for $M = 1$. Finally, for $M = 1.1$, in figure 9(f), the strongest tone at $St = 0.46$ is related to the first helical mode, whereas the two tones at $St = 0.29$ and $St = 0.66$ are associated with the axisymmetric mode. Contrary to the other jets, two oscillation modes with comparable amplitude exist. The azimuthal structure of the jets is hence affected by the Mach number.

E. Mach number variations of the near-nozzle tone properties

The Strouhal numbers of the tones in the near-nozzle pressure spectra are represented in figure 10 as a function of the Mach number. They are compared with the experimental data of Jaunet *et al.* [24] and with the Strouhal numbers predicted by relation (1) using $\langle u_c \rangle = (2/3)u_j$. The tone frequencies in the simulations are close to those predicted by the Ho & Nosseir's model (1). The dominant tones lie near the curves associated with the mode $N = 6$ for $M = 0.75$, $N = 5$ for $M = 0.8$, $N = 4$ for $M = 0.9$, $N = 3$ for $M = 1$ and $N = 5$ for $M = 1.1$. Secondary tones are related to the modes $N = 4$, 5 and 7 for $M = 0.75$, $N = 6$ for $M = 0.9$ and 1 and $N = 3$ and 7 for $M = 1.1$. As the jet Mach number increases, the frequencies switch from one curve associated with a mode N to another, highlighting a staging behaviour.

Downloaded by Christophe Bailly on June 16, 2022 | http://arc.aiaa.org | DOI: 10.2514/6.2022-2866

Downloaded by Christophe Bailly on June 16, 2022 | http://arc.aiaa.org | DOI: 10.2514/6.2022-2866

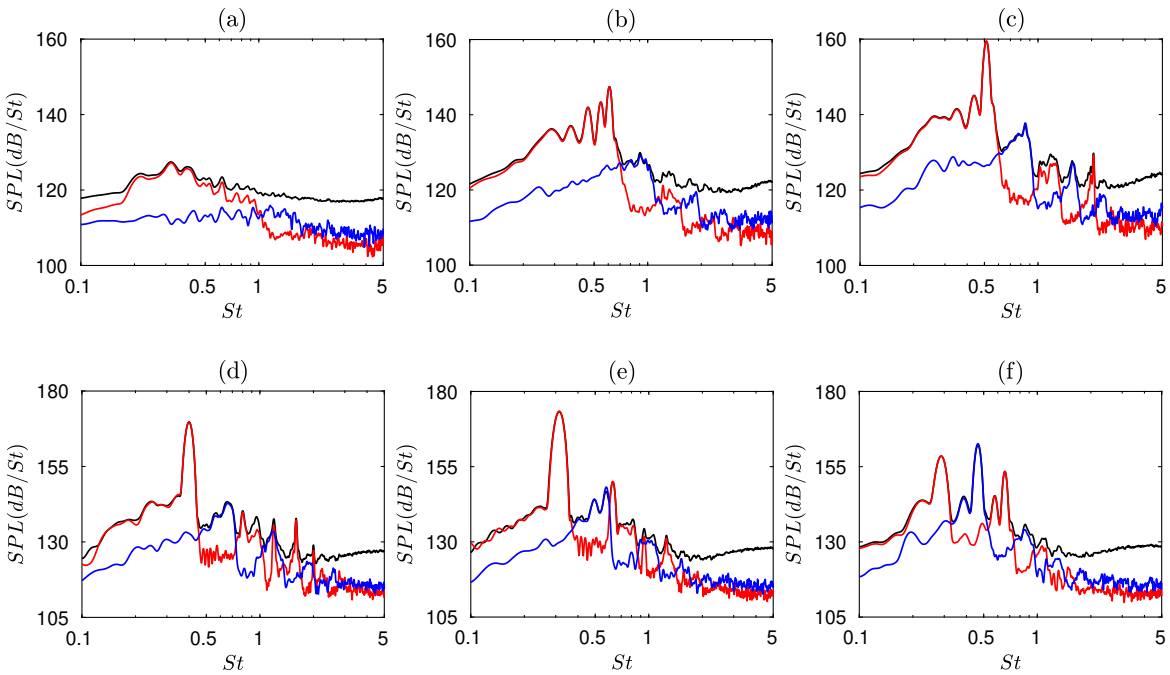

Fig. 9 Sound pressure levels (SPL) at $r = 1.5r_0$ and $z = 0$ for (a) $M = 0.6$, (b) $M = 0.75$, (c) $M = 0.8$, (d) $M = 0.9$, (e) $M = 1$ and (f) $M = 1.1$: — full signal, — $n_\theta = 0$ and — $n_\theta = 1$.

The tonal frequencies found in the experiments also lie on curves given by the model of Ho & Nosseir and jump from one mode to another, as in the simulations. Three feedback modes are observed depending on the jet Mach number. A mode $N = 3$ is visible for Mach numbers higher than 0.7, a mode $N = 6$ exists for Mach numbers between 0.85 and 1.03 and a mode $N = 5$ is present for Mach numbers higher than 0.97. For $M \leq 0.9$, the frequencies of the dominant tones in the LES are related to feedback mode orders N higher than that of the mode $N = 3$ found experimentally, whereas for higher Mach numbers, they are in agreement with those from the experiments. These discrepancies may be due to differences in the nozzle-exit velocity profiles, unknown in the experiments.

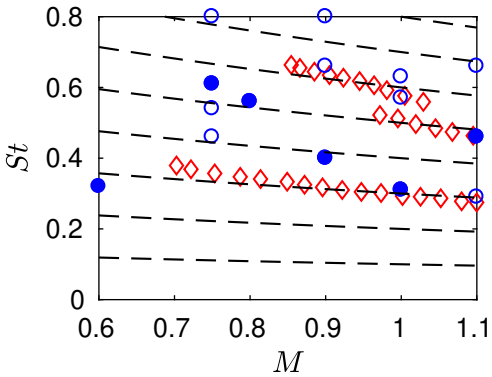

Fig. 10 Mach number variations of the near-nozzle peak frequencies: • dominant and ○ secondary tones in the LES, ◇ measurements of Jaunet *et al.* [24] and - - - relation (1)**.**

The Mach number variations of the tone frequencies are represented in figure 11 for the two first azimuthal modes separately. The frequencies predicted by the model of Ho & Nosseir are plotted using blue dashed lines. For both modes, the dominant peak frequencies are close to the frequencies given by this model, even for the jet at $M = 0.6$ with no marked resonance phenomenon. They can be associated with a feedback mode N, whose values are gathered in

table 2 for each Mach number. For a given azimuthal mode, for $M \geq 0.75$, the mode order N decreases monotonously with the jet velocity. Moreover, in figure 11, the frequency bands of the free-stream upstream-travelling guided jet waves determined using a vortex-sheet model are indicated by grey areas in order to investigate the possible closing of the feedback loops by these waves. Each grey band is related to a radial mode of the guided jet waves, with the radial mode order n_r increasing with the frequency. The dominant tones lie in the frequency range of the first radial mode for both azimuthal modes and the secondary tones are in or close to the frequency bands of the first three radial modes for $n_\theta = 0$ and of the second and third radial modes for $n_\theta = 1$. This result indicates that the free-stream upstream-propagating guided jet waves are likely to close the feedback loops. For both azimuthal modes, the frequencies of the dominant tones decrease with the Mach number, jumping from one curve related to a feedback mode N down to a lower one $N - 1$. This mode jump is explained by the closure of the feedback loops by the guided jet waves. Indeed, the frequencies of these waves for a given radial mode decay more rapidly with the Mach number than the frequencies predicted by the model of Ho & Nosseir for a given feedback mode N. As the Mach number increases, the frequency of the mode N becomes higher than the frequencies of the guided jet waves, which does not allow the closing of the loop. The loop thus cannot be closed for the mode N, but for a lower one.

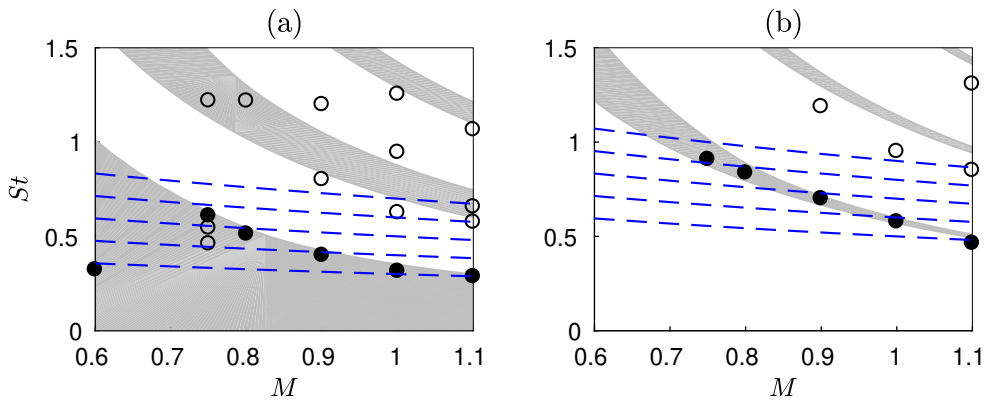

Fig. 11 Mach number variations of the Strouhal numbers of the tones in the near-nozzle pressure spectra for (a) $n_\theta = 0$ and (b) $n_\theta = 1$, • dominant and ∘ secondary tones, (grey shading) allowable frequency bands of the free-stream upstream-propagating guided jet waves, - - - Ho & Nosseir model (1) with N varying from (a) 3 to 7 and (b) 5 to 9.

Table 2 Feedback mode N related to the dominant peak frequency for $n_\theta = 0$ and $n_\theta = 1$.

M	0.6	0.75	0.8	0.9	1	1.1
$N(n_\theta = 0)$	3	6	5	4	3	3
$N(n_\theta = 1)$	/	8	8	7	6	5

The Mach number variations of the tone amplitudes are plotted in figure 12. They are compared with the typical M^8 scaling law of aerodynamic noise for subsonic jets [38], plotted in dashed blue lines. For $n_\theta = 0$ in figure 12(a), the tone amplitude increases by 45 dB between $M = 0.6$ and $M = 1$. This increase is much greater than that predicted by the M^8 law, indicating the generation of noise by a strong resonance phenomenon. For $M = 1.1$, the tone intensity is reduced by about 15 dB with respect to the level for $M = 1$. This reduction may be due to the fact that two oscillation modes with comparable amplitude are observed for the jet at $M = 1.1$, whereas the axisymmetric mode prevails for the other cases. For $n_\theta = 1$ in figure 12(b), the intensity of the dominant tone increases by 10 dB between $M = 0.75$ and $M = 1$. The variations of the tone amplitudes are much closer to the M^8 law than those for $n_\theta = 0$. For $M = 1.1$, the tone level is enhanced by 13 dB compared with that for $M = 1$. For this jet, a marked resonance is observed for $n_\theta = 1$, causing this strong increase of the tonal intensity.

Downloaded by Christophe Bailly on June 16, 2022 | http://arc.aiaa.org | DOI: 10.2514/6.2022-2866

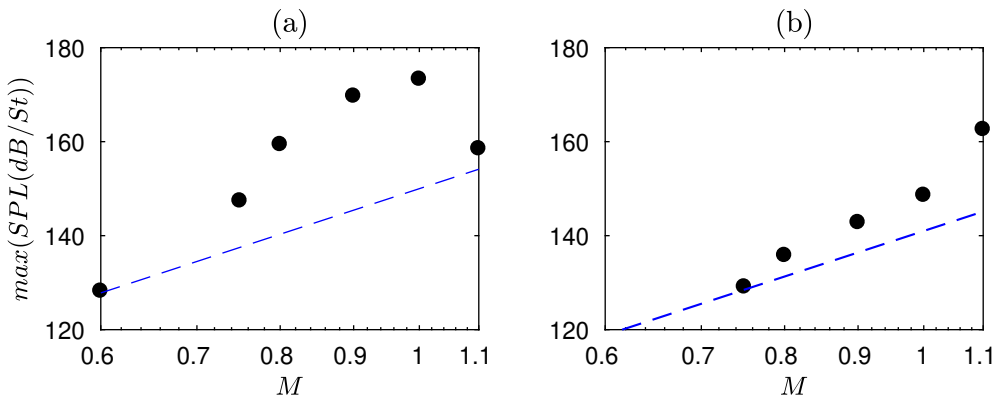

Fig. 12 Mach number variations of the amplitudes of the near-nozzle tones for (a) $n_\theta = 0$ and (b) $n_\theta = 1$, - - - M^8.

Downloaded by Christophe Bailly on June 16, 2022 | http://arc.aiaa.org | DOI: 10.2514/6.2022-2866

F. Structure of the pressure field at the tone frequencies

The structures of the jet pressure fields in the plane (z, r) at the peak frequencies for the two first azimutal modes are investigated using a Fast Fourier Transform in the time domain [10]. The amplitude fields obtained for the jets at $M = 0.6$, 0.9 and 1.1 are represented in figures 13 for $n_\theta = 0$ and in figure 14 for $n_\theta = 1$. The results for the jets at $M = 0.75$, 0.8 and 1 resemble those for $M = 0.9$. For the axisymmetric mode, for $M = 0.6$ in figure 13(a), a spot of high amplitude is found in the jet for $z \geq 4r_0$, This spot may be linked to a compression zone caused by the flow impingement on the plate. Moreover, the levels in the jet are much weaker for $z \leq 4r_0$ than farther downstream, implying that the amplitude of the upstream-travelling guided jet waves near the nozzle is low. Hence, these waves are unlikely to excite the jet shear layer, which prevents the establishment of a feedback loop. For $M = 0.9$ and 1.1 in figures 13(b,c), spots of high amplitude appear in all the jet column. They can be associated with the nodes of a standing wave establishing between the nozzle and the plate, as observed by Panda *et al.* [39] for screeching jets and by Gojon *et al.* [10, 40] for supersonic impinging jets. This standing wave is created by the superposition of the downstream-propagating jet instability waves and upstream-propagating guided jet waves. As the instability waves are linked to the vortical structures convected in the jet flow, the number of nodes of the standing wave is the same as the number of structures between the nozzle and the plate. There are 4 and 3 lobes for $M = 0.9$ and 1.1, respectively, which is in agreement with the feedback mode numbers N determined in the previous section in table 2.

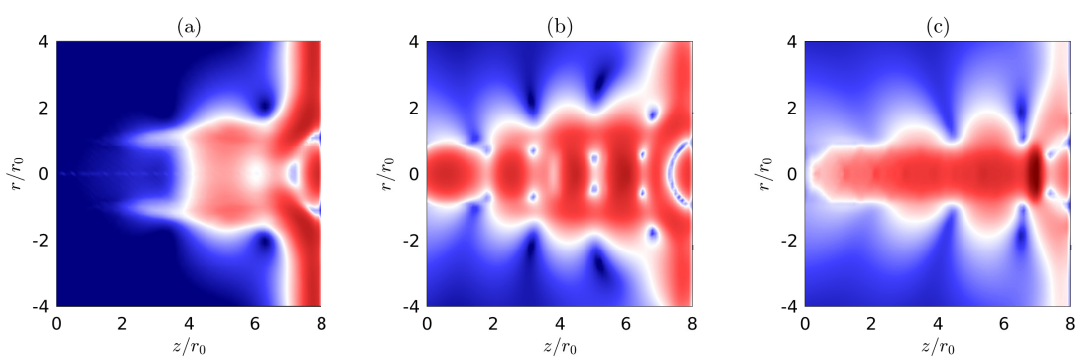

Fig. 13 Pressure levels for the axisymmetric mode at the peak frequencies (a) $St = 0.32$ for $M = 0.6$, (b) $St = 0.40$ for $M = 0.9$ and (c) $St = 0.29$ for $M = 1.1$. The color scales range from (a) 130 to 160 dB/St, (b) 150 to 200 dB/St and (c) 140 to 190 dB/St, from blue to red.

The results obtained for the first helical mode are shown in figure 14. In all cases, the amplitudes near the jet axis

are negligible, as expected for an helical oscillation mode. For $M = 0.6$ in figure 14(a), the pressure levels are highest in the shear layers. No clear structures are found in the layers, suggesting no strong feedback phenomenon at the peak frequency. For $M = 0.9$ and 1.1 in figures 14(b,c), lobes of amplitude are visible inside the jet, indicating a resonant interaction between upstream- and downstream-propagating waves. The number of lobes is equal to 5 and 7 for $M = 0.9$ and 1.1, respectively, which is consistent with the values of N found in section III.E.

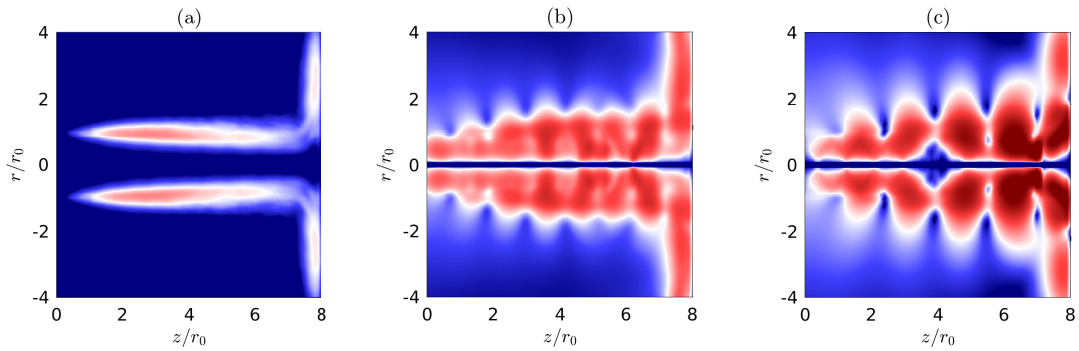

Fig. 14 Pressure levels for the first helical mode at the peak frequencies (a) $St = 1.16$ for $M = 0.6$, (b) $St = 0.7$ for $M = 0.9$ and (c) $St = 0.46$ for $M = 1.1$. The color scales range from (a) 130 to 160 dB/St, (b) 130 to 170 dB/St and (c) 150 to 180 dB/St, from blue to red.

Conclusion

In this paper, the generation of tones by impinging round jets with a Mach number varying from 0.6 to 1.1 has been investigated using large-eddy simulations. For the jet at a Mach number of 0.6, the emitted noise is broadband and weak. For higher Mach numbers, intense tones are produced by feedback loops establishing between the nozzle and the plate, consisting of downstream-propagating vortical structures and upstream-travelling pressure waves. Their frequencies are thus close to those predicted by a classical feedback model. Each tone can be associated with a feedback mode, whose order depends on the jet Mach number. As the jet Mach number varies, the tone frequencies jump from one feedback mode to another, exhibiting a staging behaviour typical of resonance phenomena. Moreover, they also lie in the allowable frequency ranges of the upstream-travelling guided jet waves, indicating that these waves close the feedback loops. A feedback mode can establish only if its frequency is located in the bands of the guided jet waves, which explains the mode jumps with the Mach number. Moreover, at each tonal frequency, the azimuthal structures of the jet oscillation modes are consistent with the axisymmetric or helical nature of the guided jet waves. For $M \leq 1$, the dominant tones are related to an axisymmetric oscillation mode, whereas for $M = 1.1$, the strongest tone is associated with the first helical mode, which shows that the Mach number affects the azimuthal structure of the jets. In further work, it could be interesting to explain why the first helical mode is stronger than the axisymmetric mode for the jet at $M = 1.1$. For this purpose, the growth rates of the Kelvin-Helmholtz waves at the tone frequencies for the two first azimuthal modes could be compared to determine which is the most amplified mode.

Acknowledgments

This work was financed by ArianeGroup and the DGA (Direction Générale de l'Armement). It was also financially supported by the IRICE IJES project RA0014963 (Installed Jet Effect Simulator, FEDER-FSE Rhône-Alpes). It was granted access to the HPC resources of PMCS2I (Pôle de Modélisation et de Calcul en Sciences de l'Ingénieur et de l'Information) of Ecole Centrale de Lyon, PSMN (Pôle Scientifique de Modélisation Numérique) of ENS de Lyon, P2CHPD (Pôle de Calcul Hautes Performances Dédié) of Université Lyon I and to the resources of IDRIS (Institut du Développement et des Ressources en Informatique Scientifique) under the allocation 2020-2a0204 made by GENCI (Grand Equipement National de Calcul Intensif. It was performed within the framework of the Labex CeLyA of Université de Lyon, operated by the French National Research Agency (grant no. ANR-10-LABX-0060/ANR-16-IDEX-0005).

Downloaded by Christophe Bailly on June 16, 2022 | http://arc.aiaa.org | DOI: 10.2514/6.2022-2866

References

[1] Wagner, F., *The sound and flow field of an axially symmetric free jet upon impact on a wall*, National Aeronautics and Space Administration, 1971.

[2] Neuwerth, G., "Acoustic feedback of a subsonic and supersonic free jet which impinges on an obstacle," *NASA Technical Translation No. F-15719*, 1974.

[3] Preisser, J. S., "Fluctuating surface pressure and acoustic radiation for subsonic normal jet impingement," *NASA Technical Paper 1361*, 1979.

[4] Ho, C.-M., and Nosseir, N. S., "Dynamics of an impinging jet. Part 1. The feedback phenomenon," *Journal of Fluid Mechanics*, Vol. 105, 1981, pp. 119–142. https://doi.org/10.1017/S0022112081003133.

[5] Nosseir, N. S., and Ho, C.-M., "Dynamics of an impinging jet. Part 2. The noise generation," *Journal of Fluid Mechanics*, Vol. 116, 1982, pp. 379–391. https://doi.org/10.1017/S0022112082000512.

[6] Powell, A., "The sound-producing oscillations of round underexpanded jets impinging on normal plates," *J. Acoust. Soc. Am.*, Vol. 83, No. 2, 1988, pp. 515–533. https://doi.org/10.1121/1.396146.

[7] Norum, T. D., "Supersonic rectangular jet impingement noise experiments," *AIAA J.*, Vol. 29, No. 7, 1991, pp. 1051–1057. https://doi.org/10.2514/3.10703.

[8] Tam, C., and Norum, T., "Impingement tones of large aspect ratio supersonic rectangular jets," *AIAA J.*, Vol. 30, No. 2, 1992, pp. 304–311. https://doi.org/10.2514/3.10919.

[9] Henderson, B., Bridges, J., and Wernet, M., "An experimental study of the oscillatory flow structure of tone-producing supersonic impinging jets," *J. Fluid Mech.*, Vol. 542, 2005, pp. 115–137. https://doi.org/10.1017/S0022112005006385.

[10] Gojon, R., Bogey, C., and Marsden, O., "Investigation of tone generation in ideally expanded supersonic planar impinging jets using large-eddy simulation," *J. Fluid Mech.*, Vol. 808, 2016, pp. 90–115. https://doi.org/10.1017/jfm.2016.628.

[11] Bogey, C., and Gojon, R., "Feedback loop and upwind-propagating waves in ideally expanded supersonic impinging round jets," *J. Fluid Mech.*, Vol. 823, 2017, pp. 562–591. https://doi.org/10.1017/jfm.2017.334.

[12] Umeda, Y., Maeda, H., and Ishii, R., "Hole tone generated from almost choked to highly choked jets," *AIAA J.*, Vol. 26, No. 9, 1988, pp. 1036–1043. https://doi.org/10.2514/3.10009.

[13] Umeda, Y., and Ishii, R., "Hole tone generation from highly choked jets," *J. Acoust. Soc. Am.*, Vol. 94, No. 2, 1993, pp. 1058–1066. https://doi.org/10.1121/1.406952.

[14] Varé, M., and Bogey, C., "Generation of acoustic tones in round jets at a Mach number of 0.9 impinging on a plate with and without a hole," *J. Fluid Mech.*, Vol. 936, 2022, p. A16. https://doi.org/10.1017/jfm.2022.47.

[15] Tam, C., and Ahuja, K., "Theoretical model of discrete tone generation by impinging jets," *Journal of Fluid Mechanics*, Vol. 214, 1990, pp. 67–87. https://doi.org/10.1017/S0022112090000052.

[16] Edgington-Mitchell, D., Jaunet, V., Jordan, P., Towne, A., Soria, J., and Honnery, D., "Upstream-travelling acoustic jet modes as a closure mechanism for screech," *Journal of Fluid Mechanics*, Vol. 855, 2018. https://doi.org/10.1017/jfm.2018.642.

[17] Mancinelli, M., Jaunet, V., Jordan, P., and Towne, A., "Screech-tone prediction using upstream-travelling jet modes," *Experiments in Fluids*, Vol. 60, No. 1, 2019, p. 22. https://doi.org/10.1007/s00348-018-2673-2.

[18] Jordan, P., Jaunet, V., Towne, A., Cavalieri, A., Colonius, T., Schmidt, O., and Agarwal, A., "Jet-flap interaction tones," *J. Fluid Mech.*, Vol. 853, 2018, pp. 333–358. https://doi.org/10.1017/jfm.2018.566.

[19] Tam, C., and Chandramouli, S., "Jet-plate interaction tones relevant to over-the-wing engine mount concept," *Journal of Sound and Vibration*, Vol. 486, 2020, p. 115378. https://doi.org/10.1016/j.jsv.2020.115378.

[20] Bogey, C., "Acoustic tones in the near-nozzle region of jets: characteristics and variations between Mach numbers 0.5 and 2," *J. Fluid Mech.*, Vol. 921, 2021. https://doi.org/10.1017/jfm.2021.426.

[21] Schmidt, O. T., Towne, A., Colonius, T., Cavalieri, A. V. G., Jordan, P., and Brès, G. A., "Wavepackets and trapped acoustic modes in a turbulent jet: coherent structure eduction and global stability," *Journal of Fluid Mechanics*, Vol. 825, 2017, pp. 1153–1181. https://doi.org/10.1017/jfm.2017.407.

Downloaded by Christophe Bailly on June 16, 2022 | http://arc.aiaa.org | DOI: 10.2514/6.2022-2866

[22] Towne, A., Schmidt, O., and Bres, G., "An investigation of the Mach number dependence of trapped acoustic waves in turbulent jets," 2019. https://doi.org/10.2514/6.2019-2546.

[23] Panickar, P., and Raman, G., "Criteria for the existence of helical instabilities in subsonic impinging jets," *Physics of Fluids*, Vol. 19, No. 10, 2007, pp. 103–106. https://doi.org/10.1063/1.2798804.

[24] Jaunet, V., Mancinelli, M., Jordan, P., Towne, A., Edgington-Mitchell, D. M., Lehnasch, G., and Girard, S., "Dynamics of round jet impingement," *AIAA Paper 2019-2769*, 2019. https://doi.org/10.2514/6.2019-2769.

[25] Bogey, C., Marsden, O., and Bailly, C., "Large-eddy simulation of the flow and acoustic fields of a Reynolds number 10^5 subsonic jet with tripped exit boundary layers," *Phys. Fluids*, Vol. 23, No. 3, 2011, p. 035104. https://doi.org/10.1063/1.3555634.

[26] Varé, M., and Bogey, C., "Flow and Acoustic Fields of Rocket Jets Impinging on a Perforated Plate," *AIAA J.*, 2022, pp. 1–14. https://doi.org/10.2514/1.J061253.

[27] Varé, M., and Bogey, C., "Presence and properties of acoustic peaks near the nozzle of impinging rocket jets," *submitted to Acta Acustica United with Acustica*, 2022.

[28] Berland, J., Bogey, C., Marsden, O., and Bailly, C., "High-order, low dispersive and low dissipative explicit schemes for multiple-scale and boundary problems," *J. Comput. Phys.*, Vol. 224, No. 2, 2007, pp. 637–662. https://doi.org/10.1016/j.jcp.2006.10.017.

[29] Bogey, C., and Bailly, C., "A family of low dispersive and low dissipative explicit schemes for flow and noise computations," *J. Computat. Phys.*, Vol. 194, No. 1, 2004, pp. 194–214. https://doi.org/10.1016/j.jcp.2003.09.003.

[30] Fauconnier, D., Bogey, C., and Dick, E., "On the performance of relaxation filtering for large-eddy simulation," *J. Turbul.*, Vol. 14, No. 1, 2013, pp. 22–49. https://doi.org/10.1080/14685248.2012.740567.

[31] Bogey, C., De Cacqueray, N., and Bailly, C., "A shock-capturing methodology based on adaptative spatial filtering for high-order non-linear computations," *J. Comput. Phys.*, Vol. 228, No. 5, 2009, pp. 1447–1465. https://doi.org/10.1016/j.jcp.2008.10.042.

[32] Tam, C., and Dong, Z., "Radiation and outflow boundary conditions for direct computation of acoustic and flow disturbances in a non uniform mean flow," *J. Comput. Acoust.*, Vol. 4, No. 02, 1996, pp. 175–201. https://doi.org/10.1142/S0218396X96000040.

[33] Bogey, C., and Bailly, C., "Three-dimensional non-reflective boundary conditions for acoustic simulations: far-field formulation and validation test cases," *Acta Acustica united with Acustica*, Vol. 88, No. 4, 2002, pp. 463–471.

[34] Mohseni, K., and Colonius, T., "Numerical treatment of polar coordinate singularities," *J. Comput. Phys.*, Vol. 157, No. 2, 2000, pp. 787–795. https://doi.org/10.1006/jcph.1999.6382.

[35] Bogey, C., De Cacqueray, N., and Bailly, C., "Finite differences for coarse azimuthal discretization and for reduction of effective resolution near origin of cylindrical flow equations," *J. Comput. Phys.*, Vol. 230, No. 4, 2011, pp. 1134–1146. https://doi.org/10.1016/j.jcp.2010.10.031.

[36] Bogey, C., "Grid sensitivity of flow field and noise of high-Reynolds-number jets computed by large-eddy simulation," *International Journal of Aeroacoustics*, Vol. 17, No. 4-5, 2018, pp. 399–424. https://doi.org/10.1177/1475472X18778287.

[37] Michalke, A., "Survey on jet instability theory," *Progress in Aerospace Sciences*, Vol. 21, 1984, pp. 159–199. https://doi.org/10.1016/0376-0421(84)90005-8.

[38] Lighthill, M., "On sound generated aerodynamically. I," *Philosophical Transactions of the Royal Society A*, Vol. 564, 1952. https://doi.org/10.1098/rspa.1952.0060.

[39] Panda, J., Raman, G., and Zaman, K., "Underexpanded screeching jets from circular, rectangular and elliptic nozzles," *AIAA Paper 1997-1623*, 1997. https://doi.org/10.2514/6.1997-1623.

[40] Gojon, R., and Bogey, C., "Flow structure oscillations and tone production in underexpanded impinging round jets," *AIAA J.*, Vol. 55, No. 6, 2017, pp. 1792–1805. https://doi.org/10.2514/1.J055618.

Downloaded by Christophe Bailly on June 16, 2022 | http://arc.aiaa.org | DOI: 10.2514/6.2022-2866